

© 2019 IEEE. Personal use of this material is permitted. Permission from IEEE must be obtained for all other uses, in any current or future media, including reprinting/republishing this material for advertising or promotional purposes, creating new collective works, for resale or redistribution to servers or lists, or reuse of any copyrighted component of this work in other works

High temperature annealing of ZnO:Al on passivating POLO junctions: Impact on transparency, conductivity, junction passivation and interface stability

Tobias F. Wietler, Byungsul Min, Sina Reiter, Yevgeniya Larionova, Rolf Reineke-Koch, Frank Heinemeyer, Rolf Brendel, Armin Feldhoff, Jan Krügener, Dominic Tetzlaff, and Robby Peibst

Abstract— We investigate the enhancement in transparency and conductivity of aluminum doped zinc oxide (ZnO:Al) layers upon high-temperature annealing and its impact on contact resistance as well as on passivation properties of carrier selective junctions based on doped polycrystalline Si on a passivating silicon oxide (POLO). The temperature stability of these junctions allows annealing of the ZnO:Al/POLO combination up to 600 °C. We prepare ZnO:Al films by DC magnetron sputtering at room temperature. We determine complex refractive index of ZnO:Al in dependence of post-deposition annealing (PDA) temperature by spectroscopic ellipsometry. High-temperature annealing improves the conductivity and reduces the absorption within ZnO:Al. The optical losses in a ZnO:Al/POLO stack are rather limited by the poly-Si layer than by the ZnO:Al. The sheet resistance improves from roughly 20000 Ω/sq for 80 nm thick as-deposited ZnO:Al films to 72 Ω/sq after fast firing at 600 °C. At the same time PDA cures the damage induced in the POLO junctions during ZnO:Al deposition. After PDA with Al_xO_y capping layers, the passivation quality even surpasses the initial level. A transmission electron microscopy analysis of the interface between the ZnO:Al and the underlying poly-Si reveals the formation of a silicon oxide like interfacial layer after PDA at 400 °C. This interfacial layer causes

a high contact resistivity of the metal/ZnO:Al/POLO-junction and could limit the thermal budget for cell processing. Our results indicate that after successful process adjustment, ZnO:Al could substitute In-based transparent conductive oxides on POLO cells for cost reasons and also enable a high efficiency potential.

Index Terms— Passivating contacts, POLO junction, polycrystalline silicon, thermal treatment, ZnO:Al

I. INTRODUCTION

WITH the enhancement of silicon surface passivation quality in during the last years, contact recombination losses become a key factor in the pursuit for highly efficient silicon solar cells. For this reason, passivating carrier-selective junctions (CSJs) become increasingly important and attract significant attention recently. [1] An already established concept to realize such junctions is the application of heterojunctions using surface passivating intrinsic and doped hydrogenated amorphous silicon (*a*-Si:H) layers on the front and rear side of the solar cell. [2, 3] An alternative with also excellent interface passivation quality is the junction between crystalline (*c*-) and polycrystalline (poly-) silicon with an embedded interfacial silicon oxide (POLO). [4, 5] Very low recombination current densities enable a conversion efficiency of 26.1% for a POLO-cell with interdigitated back contacts. [6] Over a wide range of the spectrum doped poly-Si has a lower absorption coefficient than doped *a*-Si:H, implying a significantly lower absorption loss in a poly-Si layer than in an *a*-Si:H layer with the same thickness. [7, 8, 9] For a 15 nm thick, doped poly-Si layer, for example, the parasitic absorption induces a loss in the short circuit current density of 0.75 mA/cm². For a doped *a*-Si:H layer with the same thickness, the corresponding loss is 3 mA/cm². [7] However, less than 20 nm thin poly-Si layers have sheet resistances above 1000 Ω/sq. [10] A highly conductive and transparent

Manuscript received September 21, 2017. This work was supported by the Ministry for Science and Culture of Lower Saxony, the German Ministry for Economic Affairs and Energy under grant number 0325702 (POLO) and by the European Union's Horizon 2020 research and innovation program under grant number 727529 (DISC).

T. F. Wietler, B. Min, S. Reiter, Y. Larionova, R. Reineke-Koch, F. Heinemeyer, R. Brendel, and R. Peibst are with the Institute for Solar Energy Research Hamelin (ISFH), Am Ohrberg 1, 31860 Emmertal, Germany (phone: +49 5151 999 644; fax: +49 5151 999 400; e-mail: wietler@isfh.de).

R. Brendel is with the Institute for Solid State Physics, Leibniz Universität Hannover, Appelstr. 2, 30167 Hanover, Germany.

J. Krügener and R. Peibst are with the Institute of Electronic Materials and Devices (MBE), Schneiderberg 32, 30167 Hanover, Germany.

D. Tetzlaff is with the Institute of Applied Physics, Technische Universität Braunschweig, Mendelssohnstr. 2, 38106 Braunschweig.

A. Feldhoff is with the Institute for Physical Chemistry and Electrochemistry, Leibniz Universität Hannover, Callinstr. 3A, 30167 Hannover.

layer on top of the poly-Si could help to ensure the required lateral conductivity for the transport of charge carriers towards the metallization grid on the front side. It should also provide low contact resistances with respect to the poly-Si and the metal. Besides graphene, metal nanowires or carbon nanotubes, a transparent conductive oxide (TCO) are a common choice to fulfill these requirements. [11] In the last years, different groups demonstrated double-sided POLO junction solar cells with a front-side TCO using either ITO [12, 13], ZnO:Al [14] or a double-layer of both materials [8].

With respect to the TCO, poly-Si has further advantages in comparison to *a*-Si:H. POLO junctions exhibit high temperature stability enabling deposition and post-deposition annealing (PDA) of TCOs at temperatures above 200 °C. [10] This allows for the use of ZnO:Al films with high transparency and low resistivity. [15, 16, 17] With respect to material cost, ZnO:Al is more attractive than In-based TCO layers. Furthermore, the high active doping concentration in *p*⁺ doped poly-Si layers might facilitate the formation of a low-resistivity tunnel junction to the TCO. On the other hand, POLO junctions seem to be more vulnerable by sputter damage. [18] Also, processing at elevated temperatures may affect the stability of the interface between poly-Si and ZnO:Al and lead to the formation of interlayers. [19]

In this work, we investigate the PDA of well-passivating POLO junctions combined with ZnO:Al as a TCO up to temperatures as high as 600 °C. We show that the conductivity and transparency of the ZnO:Al films strongly improve with increasing PDA temperature. We report on the impact of ZnO:Al deposition and subsequent thermal treatment on passivation quality and contact resistivity of the ZnO:Al/POLO stack. We analyze the microstructure and chemical composition of the layer stack and identify an isolating interfacial layer between ZnO:Al and poly-Si.

II. EXPERIMENTAL DETAILS

We use different characterization methods that require specific sample structures. Table I provides an overview of the sample types. The remaining part of this section presents the details of the sample preparation. We use the same conditions for ZnO:Al deposition for all samples.

We deposit ZnO:Al films by DC-magnetron sputtering in an in-line coating system (ATON 500, Applied Materials) from a rotatable ceramic ZnO/Al₂O₃ (2 wt.%) target (diameter: 160 mm). Argon (200 sccm) and oxygen (5 sccm) are used as process gases. The sputtering process operates without substrate heating. The target-substrate distance is 143 mm. Working pressure and power are 2.5×10^{-3} hPa and 2 kW, respectively. Before deposition, we perform a pre-sputtering of 10 min to remove potential contaminations from the target surface.

For spectral transmission measurements with a double-beam spectrometer (Cary 5000, Varian/Agilent Technologies) we use 25 mm × 25 mm borofloat glass substrates treated with a Radio Corporation of America (RCA) wet chemical cleaning

TABLE I





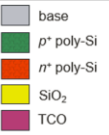
OVERVIEW OF SAMPLE TYPES				
TCO on SiO ₂ on Si	TCO on glass	Symmetrical samples		Legend
				
VASE	Transmission	Lifetime	Sheet resistance	

Table I. Overview of the sample types we prepare for the different measurements in this study. We use the same conditions for ZnO:Al deposition for all samples. We apply an Al_xO_y capping layer during PDA of cell precursors and symmetrical samples.

sequence and deposit 50 nm thick ZnO:Al layers.

For optical characterization of the ZnO by variable-angle spectroscopic ellipsometry (VASE), we prepare test structures from single-side polished planar *n*-type Czochralski silicon wafers. After an RCA cleaning sequence, a 140 nm thick SiO₂ layer is grown in a wet thermal oxidation process. Subsequently, we deposit 50 nm ZnO:Al on top of that oxide. We perform VASE measurements in the wavelength range of 240 nm to 1700 nm (M-2000UI, J.A. Woollam, Inc.). We measure the amplitude ratio Ψ and phase difference Δ of incident and reflected radiation for five angles of incidence (50°, 55°, 60°, 65°, 70° for glass substrates and 60°, 65°, 70°, 75°, 80° for silicon substrates).

Both VASE and transmission data of our ZnO:Al layers are simultaneously simulated via Kramers-Kronig consistent functions with few independent variables. [20] This model describes all our ZnO:Al films accurately as shown in Figs. 1(a) and (b) for a representative set of measured and model-fit values for amplitude ratio Ψ and phase difference Δ from a sample after PDA at 600 °C on a hot plate.

We prepare symmetrical planar *n*⁺-POLO lifetime samples using 150 μm-thick 156 mm × 156 mm pseudo-square *n*-type Czochralski (Cz) silicon wafers with a resistivity of 5 Ωcm. These wafers are RCA cleaned and covered with a 1.7 nm thick dry thermal oxide layer on both sides. We use low-pressure chemical vapor deposition (LPCVD) to deposit 25 nm of intrinsic polycrystalline silicon on both sides of the silicon wafers. Subsequently, we implant phosphorus ions at 5 keV (implant dose 2.5×10^{15} cm⁻²) on both sides of the wafer. Then these samples are annealed for 30 min (plateau) at 950 °C in a nitrogen atmosphere. In a last step, an 80 nm thin ZnO:Al layer [21] is sputtered on both sides under the above mentioned conditions. Prior to ZnO:Al deposition, a dip in 1% hydrofluoric acid has been applied for one minute to remove the native oxide. We split the finished 156 mm × 156 mm *n*⁺-POLO lifetime samples into pieces of 50 mm × 50 mm for a process parameter investigation. We evaluate the minority carrier lifetime from photo conductance decay (PCD)

measurements (Sinton WCT-120 lifetime tester) in transient and generalized mode.

To characterize the sheet resistance, we prepare symmetrical planar p^+ -samples using the same procedure as described for the lifetime samples but using ion implantation of boron difluoride at 5 keV (implant dose $2 \times 10^{14} \text{ cm}^{-2}$) on both sides of the samples. We investigate the sheet resistance of the ZnO:Al films by four point probe (4PP) measurements and by analyzing the dark conductivity using a PCD measurement system (Sinton WCT-120 lifetime tester).

We use 10 nm thick hydrogen-rich Al_xO_y as capping layer to prevent degradation of the electrical properties of the ZnO:Al films during PDA in air. [17, 22] The hydrogen-rich capping layer could also improve the electrical properties by incorporation of hydrogen atoms as shallow donors into the ZnO:Al layer. [23, 24] In addition, hydrogen has a beneficial effect on the passivation quality of POLO junctions. [10, 25] The PDA is performed either on a hot plate for 3 min at 400 °C or 600 °C, or for a few seconds in a conveyor belt furnace with set peak temperature of 600 °C. After the PDA step, we perform optical characterization, PCD and 4PP measurements.

We use planar cell precursors after PDA at 400 °C with AlO_x capping layer to determine the contact resistivity. We remove the capping layer [26] and screen print metal fingers using a low temperature paste cured at 200 °C for 10 minutes to apply the transfer length method (TLM).

Cross-sectional transmission electron microscopy (TEM) samples are prepared from cell precursors after PDA at 400 °C with AlO_x capping layer for structural investigation in a JEOL JEM 2100-F UHR microscope operated at 200 keV. We analyze the chemical composition of the TEM samples with electron energy-loss spectroscopy (EELS) and energy dispersive X-ray spectroscopy (EDXS).

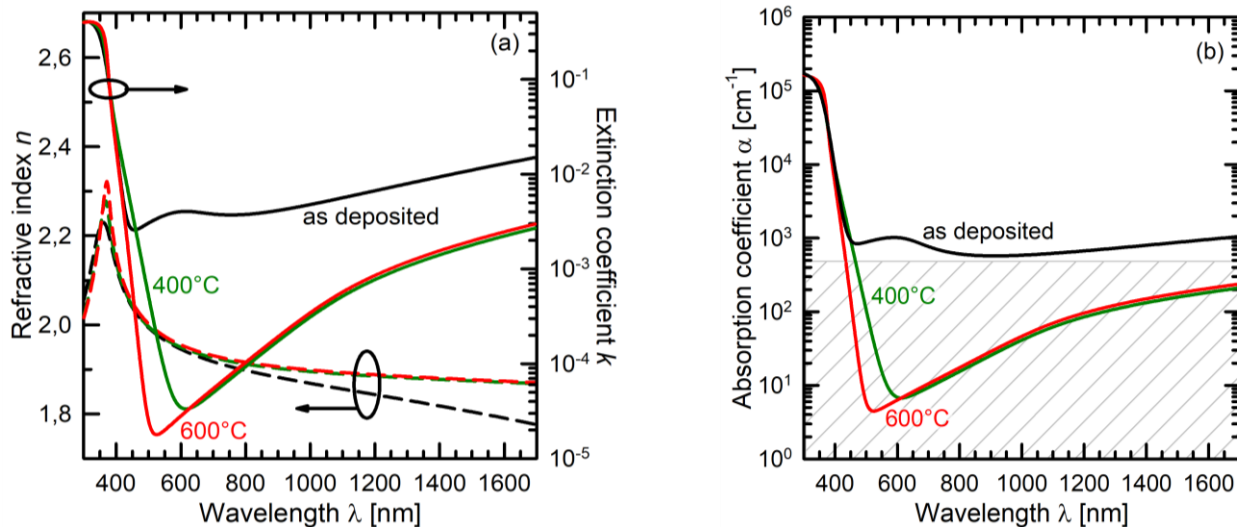


Fig. 2. (a) Optical constants n and k and (b) absorption coefficient α of ZnO:Al after deposition and after PDA at 400 °C or 600 °C on a hot plate.

TABLE II
 SIMULATED PHOTOGENERATION CURRENT DENSITY J_{photo} [mA/cm²]

	25 nm poly-Si	10 nm poly-Si	5 nm poly-Si
Simulated sample structure			
ZnO:Al (PDA: 3 min, 400 °C)	40.06	40.81	41.06
ZnO:Al (PDA: 3 min, 600 °C)	40.13	40.85	41.11
industrial PERC		41.49	

Table II. Photo-generation current density J_{photo} is calculated with the ray tracing software DAIDALOS [29] for 25 nm, 10 nm and 5 nm poly-Si thicknesses. We use experimentally determined n and k values for ZnO:Al (this work) and poly-Si [7, 9]. A PERC technology with SiN_x front side passivation and a diffused emitter serves as a benchmark. Shading of the front side and its degradation (deposition of Al₂O₃ cap) are applied for comparison. The mean square error (MSE) value of the model-fit is 4.77.

III. RESULTS AND DISCUSSION

A. Transparency

First, we evaluate the optical properties of our sputtered ZnO:Al layers and their dependence on the post-deposition annealing temperature. We extract the optical constants n and k from the analysis of the VASE and transmission data and use the k values to calculate the absorption coefficient $\alpha = 4\pi k/\lambda$ of our ZnO:Al. Figure 2 shows the spectra resulting for n , k , and α after different PDA processes. For small values of k , we obtain the absorption coefficient data using the model functions and not by direct measurement. In Fig. 2(b), the hatched area indicates the respective data range. The absorption spectrum of the as deposited ZnO:Al film shows a peak around 600 nm which is typical for ZnO:Al layers sputtered close to room temperature and caused by oxygen vacancies or zinc interstitials. [27, 28] The absorption coefficient of the ZnO:Al annealed at 400 °C and 600 °C decreases significantly in the wavelength range below 600 nm which is extremely important for good optical properties at the front contact junction of a solar cell.

Ray tracing simulations quantify the impact of the absorption in our ZnO:Al/POLO stacks on the photo-generation in the c -Si absorber. We use the ray-tracing program DAIDALOS [29] with a c -Si wafer thickness of 170 μ m. We assume a standard random pyramid textured front side and a planar rear surface. We suppose a 1.5 nm SiO₂ / n^+ -poly-Si / 80 nm ZnO:Al layer stack for the front side and a 1.5 nm SiO₂ / p^+ -poly-Si / 80 nm ZnO:Al layer stack for the rear side with three different poly-Si thicknesses: 25 nm, 10 nm, and 5 nm. An industrial type PERC technology with 75 nm SiN_x front surface passivation, a 5 nm AlO_x / 75 nm SiN_x, rear side passivation and 1 μ m Al rear side metallization serves as a reference cell. [30] Table II shows the results of

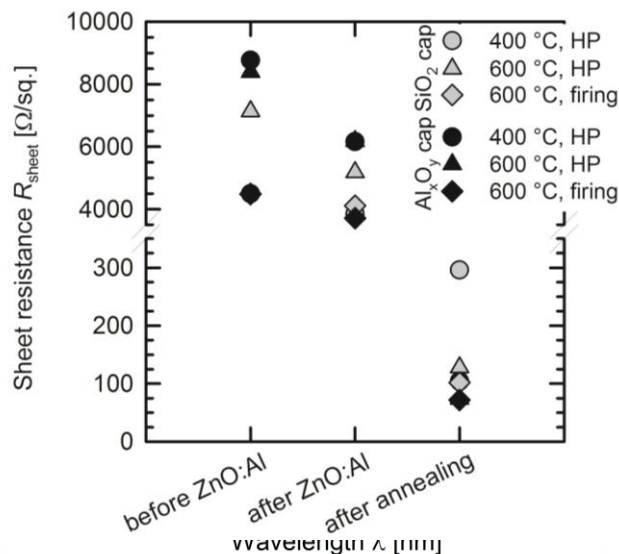


Fig. 3. Sheet resistance R_{sheet} of ZnO:Al on p^+ -POLO junctions (dark conductivity from PCD measurements). Before ZnO:Al deposition the measurements show the high sheet resistance of the thin p^+ poly-Si films. With the ZnO:Al layers deposited the combined sheet resistance of TCO and poly-Si is still high. R_{sheet} drops from several k Ω /sq to around 100 Ω /sq upon annealing on a hot plate (HP) for 3 minutes or in a fast firing furnace.

these simulations whereby the photo generation current density corresponds to a maximum of the short circuit current density. It can easily be seen that thanks to the low absorption of the ZnO:Al after PDA, the optical losses are rather limited by the poly-Si layer than by the ZnO:Al layer. With a 5 nm poly-Si thickness the photo-generated current density is only 0.38 mA/cm² lower than for the PERC reference. At the same time, the expected open-circuit voltage will be several 10 mV higher due to the excellent passivation of the POLO junctions.

B. Conductivity

We investigate the development of the sheet resistance of our ZnO:Al films after PDA. Figure 3 summarizes the sheet resistance values R_{sheet} for our ZnO:Al layers extracted from PCD measurements. The thin p^+ poly-Si layers alone have a high sheet resistance of several k Ω /sq. After TCO deposition the combined sheet resistance of the ZnO:Al layer and the p^+ poly-Si film underneath is still in the same range. This points to a low conductivity of the as-deposited ZnO:Al films. A simple estimation of the sheet resistance assuming a constant poly-Si conductivity in parallel to the as-deposited ZnO:Al layer yields about 20 k Ω /sq. After PDA, the sheet resistance has dropped remarkably to values around 100 Ω /sq. The conductivity of the p^+ poly-Si is determined by the high temperature junction formation step at 950 °C described in section II. Hence, it is stable under annealing up to 600 °C. Even if we consider a possible deactivation of the boron in the poly-Si due to diffusion of dopant atoms to the grain boundaries [31] and/or the temperature dependence of the solid solubility of boron in silicon, the PDA step could only lead to a reduced conductivity of the poly-Si. Thus, the drop in sheet resistance results from an increased conductivity in the ZnO:Al layers. The 4PP (not shown here) and PCD data

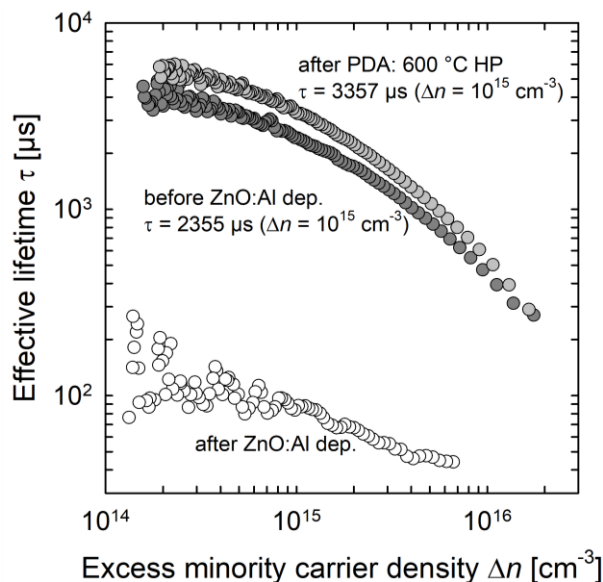


Fig. 4. Impact of ZnO:Al deposition and PDA (600 °C on a hot plate) on passivation quality of n^+ -POLO lifetime samples as measured by PCD. PDA helps to recover the initial passivation quality.

measured after PDA are in a good agreement. This is because the ZnO:Al layer provides the entire conductivity. We achieve low sheet resistance values down to 72 Ω/sq for our 80 nm thin ZnO:Al layers after annealing at 600 °C. PDA at 400 °C results in sheet resistance values down to 102 Ω/sq . The rapid annealing in a firing furnace works just as well as the hot plate annealing. The final R_{sheet} values correspond to a sufficient lateral conductivity for front-side application.

C. Impact on passivation quality

We study the impact of processing ZnO:Al/capping layer stacks on the passivation quality of POLO junctions. We use planar lifetime samples with n^+ -POLO junctions on the front and rear side. We perform PCD measurements before and after ZnO:Al deposition. As a first result, we observe a decrease of the surface passivation quality after the ZnO:Al sputtering process (Fig. 4, after ZnO:Al deposition). For $a\text{-Si:H}/c\text{-Si}$ junctions, it is well known that sputtering damage can be cured by an annealing step. [32, 33] We apply the annealing conditions described above: 3 minutes at 400 °C or 600 °C on a hot plate (HP) and a firing step with a peak temperature at 600 °C in a belt furnace.

For all annealing conditions investigated, the effective lifetimes τ_{eff} , implied open circuit voltages iV_{oc} , and implied pseudo fill factor values $ipFF$ after PDA equal or even exceed the initial values prior to ZnO:Al deposition. Figure 4 exemplifies the result after PDA at 600 °C on a hot plate. We attribute this to the beneficial effect of hydrogen from the AlO_x capping layer on the passivation quality of POLO junctions. This finding is consistent with previous reports from our group [10] and others [25]. The final values for the lifetime sample shown in Fig. 4 are: $\tau_{\text{eff}} = 3357 \mu\text{s}$ at an excess minority carrier density of $\Delta n = 10^{15} \text{cm}^{-3}$, $iV_{\text{oc}} = 718 \text{mV}$, and $ipFF = 84.9 \%$.

On single-side textured cell precursors with optimized

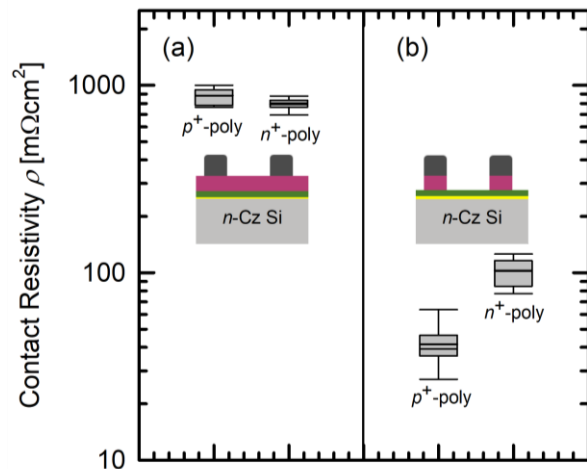


Fig. 5. Contact resistivity of metal/ZnO:Al/POLO stacks after PDA at 400 °C with AlO_x capping layer. Measurements of the metal/ZnO:Al/POLO stack as indicated in Fig. 5(a) detect primarily the contact resistivity between the ZnO:Al and the metal due to the high conductivity of the ZnO:Al layer. After TCO removal between the contact fingers the TLM results give information about the ZnO:Al/POLO contact resistivity (Fig. 5(b)). The major contribution to the contact resistance originates from the ZnO:Al/POLO-junction.

POLO-junctions, we achieve iV_{oc} values up to 747 mV after ZnO:Al sputtering and PDA.

D. Contact resistivity

Besides transparency and conductivity, a low contact resistivity of the metal/TCO/CSJ-system is essential for a highly efficient solar cell. Processing at elevated temperatures may affect the stability of the interface between poly-Si and ZnO:Al and result in the formation of possibly insulating interlayers. [19] We investigate the contact resistivity of samples after PDA at 400 °C. This temperature already yields enhanced transparency, conductivity and surface passivation, while we observe only slight additional improvements for PDA at 600 °C. TLM measurements of the metal/ZnO:Al/POLO stack as indicated in Fig. 5(a) detect primarily the contact resistivity between the ZnO:Al and the metal due to the high conductivity of the ZnO:Al layer compared to the poly-Si. We obtain $42 \pm 11 \text{m}\Omega\text{cm}^2$ and $102 \pm 17 \text{m}\Omega\text{cm}^2$ for p^+ - and n^+ -POLO, both on n -type substrates. After TCO removal between the contact fingers the TLM results give information about the ZnO:Al/POLO contact resistivity (see Fig. 5(b)). We measure even higher values of $935 \pm 96 \text{m}\Omega\text{cm}^2$ for the metal/ZnO:Al/ p^+ -POLO stack and $808 \pm 50 \text{m}\Omega\text{cm}^2$ for the metal/ZnO:Al/ n^+ -POLO stack.

The POLO junction itself shows a remarkably low contact resistivity [34]. Hence, the major contribution to the contact resistance of the complete stack originates from the ZnO:Al/POLO-junction, even if we consider that the latter is a full area contact, in contrast to the metal/ZnO:Al contact with an area fraction of about 3 %. Thus, we focus on the structural analysis of the ZnO:Al/poly-Si interface to resolve the cause of its high contact resistivity.

High-resolution TEM in cross-section (see Fig. 6) reveals an

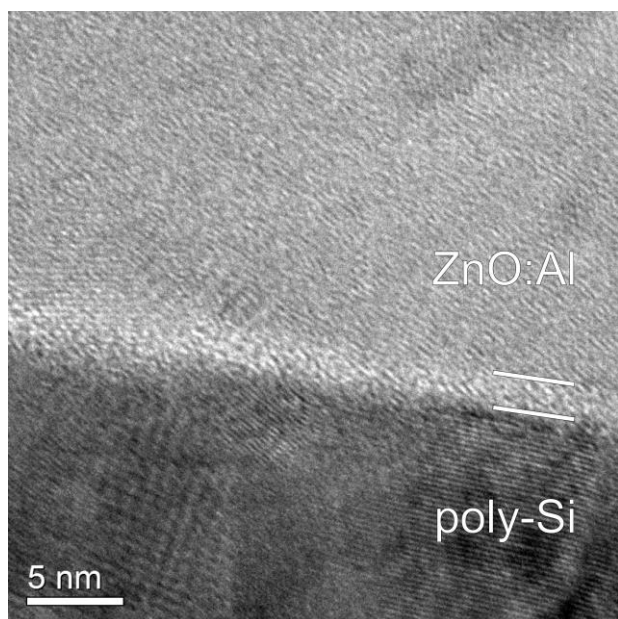


Fig. 6. High-resolution TEM micrograph of the interface region between poly-Si and ZnO:Al. The parallel white lines indicate an amorphous region of 2-3 nm thickness at the interface.

amorphous layer between ZnO:Al and poly-Si. The thickness of this layer is 2–3 nm. An insulating film of that thickness would clearly deteriorate the contact resistivity of the whole layer stack. We analyze the composition of the amorphous interlayer by EDXS and EELS. The EDXS profiles in Fig. 7 show an oxygen peak at the poly-Si/c-Si interface. This indicates the position of the POLO-junction oxide layer. A

second oxygen peak appears at the interface between ZnO:Al and poly-Si. This points to an oxide-like interlayer. We observe a higher mass fraction of oxygen in the interlayer than in the ZnO:Al. In addition, the position of the interlayer oxygen peak is closer to the poly-Si region than to the falling edge of the Zn profile. Another feature in Fig. 7 is the aluminum peak in the ZnO:Al region close to the interface between ZnO:Al and poly-Si, which could indicate diffusion of Zn into the poly-Si. [19] Figure 8 shows EEL spectra measured along a line from the ZnO:Al into the poly-Si with higher spatial resolution than in EDXS. The decrease of the oxygen signal around 530 eV occurs about 2 nm closer to the silicon region than the decrease of the zinc signal around 1100 eV. This is in good agreement with the findings from the EDXS profiles. We thus conclude that the amorphous interfacial layer between ZnO:Al and poly-Si is silicon oxide like. It contains only a small amount of Zn, if any. The formation of a 2–3 nm thick silicon oxide film could explain the high contact resistivity observed in our TLM data.

Such interfacial layers could result from (i) an oxide film that is present already before the ZnO:Al deposition or (ii) an initial oxidation of the polycrystalline silicon during the ZnO:Al deposition process. Further, during the PDA elevated temperatures could trigger (iii) a reduction of the zinc oxide and an oxidation of the silicon underneath or (iv) a reaction of silicon with oxygen containing species (e.g. OH-groups). The latter could either be incorporated in the ZnO:Al during deposition or diffuse through the ZnO:Al film from the ambient during PDA.

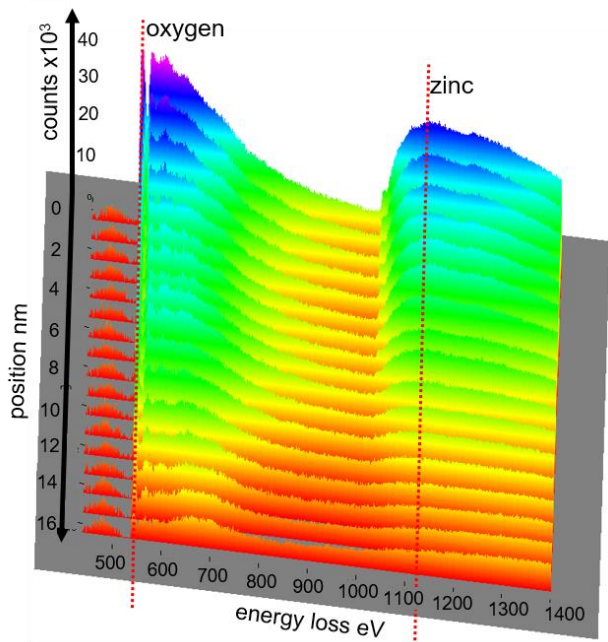


Fig. 8. EEL spectra measured along a line from the ZnO:Al (at position 0 nm) into the poly-Si with a point-to-point distance of 1 nm. The increase of the oxygen-K signal (onset energy 530 eV) occurs about 2 nm closer to the silicon than the increase of the zinc-L signal (onset energy 1020 eV). This confirms the oxide-like character of the amorphous interlayer.

We exclude the first option because the samples underwent an HF-dip prior to loading into the deposition chamber. The thickness of the native oxide formed thereafter without substrate heating should be less than 2 nm. Option (iii), the reduction of zinc oxide, should be negligible at PDA temperatures of 400 °C [19]. On the other hand, atomic hydrogen can promote the reduction of ZnO. [19] With the AlO_x capping layer acting as a hydrogen source during PDA, this could provoke the reduction of ZnO. The free Zn would then diffuse into the poly-Si layer leaving an Al enriched region close to the ZnO:Al/poly-Si interface as it was reported in [19] for annealing at temperatures above 600 °C. This would explain the Al peak in our EDXS profile. The free oxygen would then form an isolating SiO_x interlayer. With respect to options (ii) and (iv), sputtering deposition from a ceramic oxide target yields oxygen-containing species. [35, 36] These species can cause an initial oxidation of the poly-Si surface. [35] They could also be incorporated into the deposited layer, e.g. at grain boundaries, and react with the poly-Si during PDA.

Consequently, tuning of the sputtering process parameters and adjustment of the PDA conditions are the most promising ways to prevent interfacial oxide layer formation. The PDA should involve the smallest possible thermal budget and an inert atmosphere like N_2 or even vacuum conditions. A sputtering process without additional oxygen is highly desirable. A reduction of sputter damage can decrease the amount of hydrogen required to recover the passivation quality of the POLO junction and minimize the risk of ZnO reduction.

IV. CONCLUSION AND OUTLOOK

With the high thermal stability of POLO junctions it is possible to apply TCOs like ZnO:Al that require elevated temperatures either for deposition or in PDA processes. We have investigated the optical and electrical properties of ZnO:Al layers, which have passed through a PDA process with temperatures up to 600 °C. Based on detailed optical characterization by variable-angle spectroscopic ellipsometry and transmission measurements, we determined the optical constants n and k of our ZnO:Al layers. After annealing, the corresponding absorption coefficient of our ZnO:Al layers is significantly reduced. Ray tracing simulations reveal that, thanks to the low absorption of the ZnO:Al after PDA, the optical losses in a ZnO:Al/POLO stack are rather limited by the poly-Si layer than by the TCO. With a 5 nm poly-Si thickness the photo-generated current density is only 0.38 mA/cm² lower than for an industrial PERC solar cell. These excellent optical properties of our annealed ZnO:Al layers are accompanied by a sufficiently high conductivity resulting in $R_{\text{sheet}} = 72 \Omega/\text{sq}$ for a ZnO:Al thickness of 80 nm even after a few seconds firing at 600 °C. The PDA step also helps to recover the passivation quality of the POLO junction after ZnO:Al sputtering. However, we observed the formation of a silicon oxide like interfacial layer between the ZnO:Al and

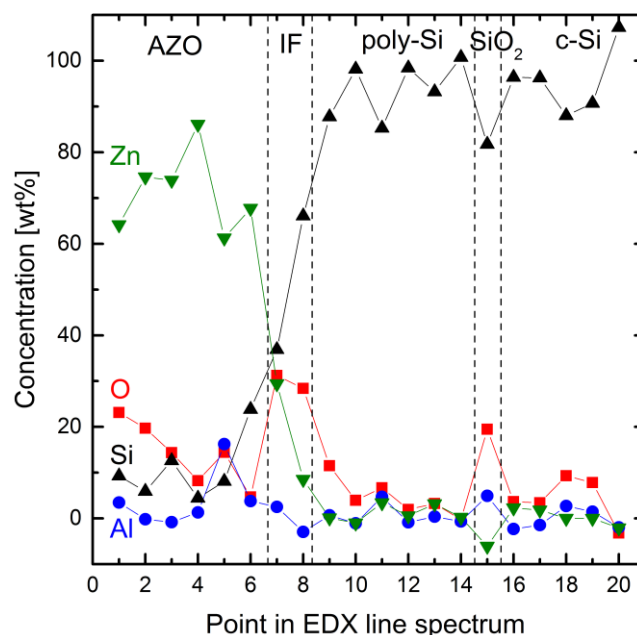


Fig. 7. EDXS line scan measured with a point-to-point distance of 3.5 nm from the ZnO:Al (at position 0) across the poly-Si into the c-Si substrate. The profiles are determined from the K-lines of Si, O and Al, as well as the L-line of Zn. An oxygen peak in the silicon region (around position 15) marks the position of the POLO-junction oxide at the poly-Si/c-Si interface. An even stronger oxygen peak is observed at the ZnO:Al/poly-Si interface indicated by the transition from Zn to Si (position 7 to 9). This peak shows the oxide-like character of the amorphous interlayer.

the underlying poly-Si after PDA at 400 °C. This interfacial layer is the origin of the high contact resistivity of the metal/ZnO:Al/POLO contact and could limit the thermal budget. Our results indicate that after successful adjustment of TCO processing, ZnO:Al could substitute In-based TCOs on POLO cells for cost reasons and also enable a high efficiency potential.

ACKNOWLEDGMENT

We thank B. Gehring and R. Winter for their help with sample processing, A. Lissel for TEM sample preparation and M. Steinbach for operating the analytical TEM.

REFERENCES

- [1] A. Cuevas, T. Allen, J. Bullock, Y. Wan, D. Yan, and X. Zhang, "Skin care for healthy silicon solar cells", *Proceedings of the 42nd IEEE PVSC*, pp. 1–6, 2015.
- [2] K. Yamamoto, D. Adachi, H. Uzu, T. Uto, T. Irie, M. Hino, M. Kanematsu, H. Kawasaki, K. Konishi, R. Mishima, K. Nakano, T. Terashita, K. Yoshikawa, M. Ichikawa, T. Kuchiyama, T. Suezaki, T. Meguro, N. Nakanishi, M. Yoshimi, D. Schroos, N. Valckx, N. Menou, and J. L. Hernández, "Progress and challenges in thin-film silicon photovoltaics: heterojunctions and multijunctions", *Proceedings of the 31st EUPVSEC*, pp. 1003–1005, 2015.
- [3] R. V. K. Chavali, S. De Wolf, and M. U. Alam, "Device physics underlying silicon heterojunction and passivating-contact solar cells: A topical review", *Progress in Photovoltaics Research and Applications*, vol. 26, pp. 241–260, 2018.
- [4] R. Brendel, T. Dullweber, R. Gogolin, H. Hannebauer, N.-P. Harder, J. Hensen, S. Kajari-Schröder, R. Peibst, J. H. Petermann, U. Römer, J. Schmidt, H. Schulte-Huxel, and V. Steckenreiter,

- “Recent progress and options for future crystalline silicon solar cells”, *Proceedings of the 28th EUPVSEC*, pp. 676-690, 2013.
- [5] F. Feldmann, M. Bivour, C. Reichel, M. Hermle, and S. W. Glunz, “Passivated rear contacts for high-efficiency n-type Si solar cells providing high interface passivation quality and excellent transport characteristics”, *Solar Energy Materials and Solar Cells*, vol. 120, pp. 270–274, 2013.
- [6] F. Haase, C. Klamt, S. Schäfer, A. Merkle, M. Rienäcker, J. Krügener, R. Brendel, and R. Peibst, “Laser Contact Openings for Local Poly-Si-Metal Contacts”, *8th SiliconPV*, Lausanne, Switzerland, 18-20.03.2018.
- [7] S. Reiter, N. Koper, R. Reineke-Koch, Y. Larionova, M. Turcu, J. Krügener, D. Tetzlaff, T. Wietler, U. Höhne, J.-D. Kähler, R. Brendel, and R. Peibst, “Parasitic absorption in polycrystalline Si-layers for carrier-selective front junctions”, *Energy Procedia*, vol. 92, pp. 199 – 204, 2016.
- [8] F. Feldmann, C. Reichel, R. Müller, and M. Hermle, “The application of poly-Si/SiO_x contacts as passivated top/rear contacts in Si solar cells”, *Solar Energy Materials and Solar Cells*, vol. 159, pp. 265–271, 2017.
- [9] B. Min, M. Vogt, T. Wietler, R. Reineke-Koch, B. Wolpensinger, E. Köhnen, D. Tetzlaff, C. Schinke, K. Bothe, R. Brendel, and R. Peibst, “Increasing the photo-generated current in solar cells with passivating contacts by reducing the poly-Si deposition temperature”, *8th SiliconPV*, Lausanne, Switzerland, 18-20.03.2018.
- [10] R. Peibst, Y. Larionova, S. Reiter, M. Turcu, R. Brendel, D. Tetzlaff, J. Krügener, T. Wietler, U. Höhne, J.-D. Kähler, H. Mehlich, and S. Frigge, “Implementation of n⁺ and p⁺ poly junctions on front and rear side of double-side contacted industrial silicon solar cells”, *Proceedings of the 32nd EUPVSEC*, pp. 323–327, 2016.
- [11] K. Ellmer, “Past achievements and future challenges in the development of optically transparent electrodes”, *Nature Photonics*, vol. 6, pp. 809-817, 2012.
- [12] R. Peibst, Y. Larionova, S. Reiter, T. F. Wietler, N. Orlowski, S. Schäfer, B. Min, M. Stratmann, D. Tetzlaff, J. Krügener, U. Höhne, J.-D. Kähler, H. Mehlich, S. Frigge, and R. Brendel, “Building blocks for industrial, screen-printed double-side contacted POLO cells with highly transparent ZnO:Al layers”, *IEEE Journal of Photovoltaics*, vol. 8, pp. 719-725, 2018.
- [13] U. Römer, R. Peibst, T. Ohrdes, B. Lim, J. Krügener, E. Bugiel, T. Wietler, R. Brendel, “Recombination behavior and contact resistance of n⁺ and p⁺ poly-crystalline Si/mono-crystalline Si junctions,” *Solar Energy Materials and Solar Cells*, Vol. 131, pp. 85-91 2014.
- [14] A. B. Morales-Vilches, Y. Larionova, T. Wietler, A. Cruz, L. Korte, R. Peibst, R. Brendel, R. Schlattmann, and B. Stannowski, “ZnO:Al/a-SiO_x front contact for polycrystalline-silicon-on-oxide (POLO) solar cells”, *AIP Conference Proceedings* vol. 1999, pp. 040016, 2018.
- [15] K. Y. Lee, C. Becker, M. Muske, F. Ruske, S. Gall, and B. Rech, “Temperature stability of ZnO:Al film properties for poly-Si thin-film devices”, *Applied Physics Letters*, vol. 91, pp. 241911, 2007.
- [16] M. Wimmer, F. Ruske, S. Scherf, and B. Rech, “Improving the electrical and optical properties of DC-sputtered ZnO:Al by thermal post deposition treatments”, *Thin Solid Films*, vol. 520, pp. 4203–4207, 2012.
- [17] F. Ruske, M. Roczen, K. Lee, M. Wimmer, S. Gall, J. Hüpkes, D. Hrunski, and B. Rech, “Improved electrical transport in Al-doped zinc oxide by thermal treatment”, *Journal of Applied Physics*, vol. 107, pp. 013708, 2010.
- [18] D. Gerlach, M. Wimmer, R. G. Wilks, R. Félix, F. Kronast, F. Ruske, and M. Bär, “The complex interface chemistry of thin-film silicon/zinc oxide solar cell structures”, *Physical Chemistry Chemical Physics*, vol. 16, p. 26266, 2014.
- [19] N. Ehrmann and R. Reineke-Koch, “Ellipsometric studies on ZnO:Al thin films: Refinement of dispersion theories”, *Thin Solid Films*, vol. 519, pp. 1475–1485, 2010.
- [20] Deok-Kyu Kim and Hong Bae Kim, “The reason of degradation in electrical properties of ZnO:Al thin films annealed with various post-annealing temperature”, *Current Applied Physics*, vol. 13, pp. 2001-2004, 2013.
- [21] Ray-tracing simulations (not shown here) based on the optical parameters obtained in this study show that 80 nm is the optimum ZnO:Al thickness for use as an anti-reflection coating.
- [22] Fang-Hsing Wang, Hung-Peng Chang, Chih-Chung Tseng, Chia-Cheng Huang, and Han-Wen Liu, “Influence of hydrogen plasma treatment on Al-doped ZnO thin films for amorphous silicon thin film solar cells”, *Current Applied Physics*, vol. 11, pp. 12-16, 2011.
- [23] C. G. Van de Walle, “Hydrogen as a cause of doping in zinc oxide”, *Physical Review Letters*, vol. 85, pp. 1012-1015, 2000.
- [24] D. Young, W. Nemeth, V. LaSalvia, M. R. Page, S. Theingi, J. Aguiar, B. G. Lee, and P. Stradins, “Low-cost plasma immersion ion implantation doping for interdigitated back passivated contact (IBPC) solar cells”, *Solar Energy Materials and Solar Cells*, vol. 158, pp. 68-76, 2016.
- [25] K. G. Sun, Y. V. Li, D. B. Saint John, and T. N. Jackson, “pH-controlled selective etching of Al₂O₃ over ZnO”, *ACS Applied Materials & Interfaces*, vol. 6, pp. 7028-7031 (2014).
- [26] S. B. Zhang, S. H. Wei, and A. Zunger, “Intrinsic n-type versus p-type doping asymmetry and the defect physics of ZnO”, *Physical Review B*, vol. 63, p. 075205, 2001.
- [27] S. Tüzemen, G. Xiong, J. Wilkinson, B. Mischuck, K. B. Ucer, and R. T. Williams, “Production and properties of p-n junctions in reactively sputtered ZnO”, *Physica B*, vol. 308, pp. 1197-1200, 2001.
- [28] H. Holst, M. Winter, M. R. Vogt, K. Bothe, M. Köntges, R. Brendel, P. P. Altermatt, “Application of a new ray tracing framework to the analysis of extended regions in Si solar cell modules”, *Energy Procedia*, vol. 38, pp. 86-93, 2013.
- [29] T. Dullweber, H. Hannebauer, U. Baumann, T. Falcon, K. Bothe, S. Steckemetz, R. Brendel, “Fine-line printed 5 busbar PERC solar cells with conversion efficiencies beyond 21%”, *Proceedings of the 29th EUPVSEC*, pp. 621-626, 2014.
- [30] J. Krügener, D. Tetzlaff, Y. Larionova, Y. Barnscheidt, S. Reiter, M. Turcu, R. Peibst, J.-D. Kähler, T. Wietler, “Electrical deactivation of boron in p⁺-poly/SiO_x/crystalline silicon passivating contacts for silicon solar cells”, *Proceedings of the 21st International Conference on Ion Implantation Technology (IIT)*, Tainan, Taiwan, 26.-30.09.2016.
- [31] D. Zhang, A. Tavakoliyaraki, Y. Wu, R. A. C. M. M. van Swaaij, and M. Zeman, “Influence of ITO deposition and post annealing on HIT solar cell structures”, *Energy Procedia*, vol. 8, pp. 207–213, 2011.
- [32] B. Demareux, S. De Wolf, A. Descoedres, Z. C. Holman, and C. Ballif, “Damage at hydrogenated amorphous/crystalline silicon interfaces by indium tin oxide overlayer sputtering”, *Applied Physics Letters*, vol. 101, pp. 171604, 2012.
- [33] M. Rienäcker, M. Bossmeyer, A. Merkle, U. Römer, F. Haase, J. Krügener, R. Brendel, and R. Peibst, “Junction resistivity of carrier-selective polysilicon on oxide junctions and its impact on solar cell performance”, *IEEE Journal of Photovoltaics*, vol. 7, p. 11, 2017.
- [34] U. Meier, and C. Pettenkofer, “Morphology of the Si–ZnO interface”, *Applied Surface Science*, vol. 252, pp. 1139–1146, 2005.
- [35] K. Ellmer, “Magnetron sputtering of transparent conductive zinc oxide: relation between the sputtering parameters and the electronic properties”, *Journal of Physics D: Applied Physics*, vol. 33, pp. R17–R32, 2000.